# Semi-empirical modelling of a variable speed scroll compressor with vapour injection

*Laurent Dardenne* [a], *Enrico Fraccari* [b], *Alessandro Maggioni* [c], *Luca Molinaroli* [c,*], *Luca Proserpio* [c], *Eric Winandy* [a]

[a] *Emerson Climate Technologies, Rue des Trois Bourdons 27, 4840, Welkenraedt, Belgium*
[b] *Emerson Climate Technologies, Pascalstraβe 65, 52076, Aachen, Germany*
[c] *Dipartimento di Energia, Politecnico di Milano, Via Lambruschini 4, 20156, Milano, Italy*

Received 2 December 2014
Received in revised form
2 March 2015
Accepted 3 March 2015
Available online 12 March 2015

## 1. Introduction

Scroll compressors are widely used in air conditioning and refrigeration industry due to their many positive characteristics such as few moving parts, low torque variation, low level of noise and vibration, high efficiency, high reliability and tolerance to refrigerant droplets. The scroll was invented by Creux (1905) at the beginning of 20th century but, due to the very small tolerances required for its manufacturing, it has been possible to start large scale production only in the seventies. Since then, many studies have been carried out to

* *Corresponding author*. Tel.: +39 02 23993872; fax: +39 02 23993913.
E-mail address: luca.molinaroli@polimi.it (L. Molinaroli).

**Nomenclature**

| | |
|---|---|
| $A$ | Area [$m^2$] |
| $BVR$ | Built-in volume ratio [dimensionless] |
| $c_P$ | Isobaric specific heat [J $kg^{-1}$ $K^{-1}$] |
| $f$ | Rotational frequency [Hz] |
| $h$ | Enthalpy [J $kg^{-1}$] |
| $\dot{m}$ | Mass flow rate [kg $s^{-1}$] |
| $NTU$ | Number of transfer unit [dimensionless] |
| $p$ | Pressure [kPa] |
| $\dot{Q}$ | Heat transfer rate [W] |
| $s$ | Entropy [J $kg^{-1}$ $K^{-1}$] |
| $T$ | Temperature [K] |
| $UA$ | Overall heat transfer coefficient [W $K^{-1}$] |
| $\dot{V}$ | Volumetric flow rate [$m^3$ $s^{-1}$] |
| $\dot{W}$ | Work transfer rate [W] |

*Greek symbols*

| | |
|---|---|
| $\alpha$ | Coefficient of proportionality in losses expression [dimensionless] |
| $\gamma$ | Ratio of isobaric to isochoric specific heat capacity [dimensionless] |
| $\varepsilon$ | Effectiveness [dimensionless] |
| $\rho$ | Density [W $m^{-3}$] |

*Subscripts*

| | |
|---|---|
| 1…9 | Refrigerant state |
| ADP | Adapted conditions |
| AMB | Ambient |
| CALC | Calculated |
| COMP | Compressor |
| CRIT | Critical |
| DIS | Discharge |
| EXP | Measured experimentally |
| INJ | Injection |
| INT | Internal |
| LEAK | Leakage |
| LOSS | Lost |
| REF | Reference or refrigerant |
| SUC | Suction |
| THR | Throat |
| VCi | i-th Virtual Compressor |
| W | Wall |

improve the compressor performance resulting in advanced technologies such as variable speed, liquid and vapour injection or flooded compression. Among them, the technology of refrigerant injection has gained increasing attention in high temperature lift application due to its inherent benefits such as the increase of system capacity (Wang et al., 2009c; Xu et al., 2013), the intrinsic modulation of system capacity trough injected refrigerant mass flow rate variation (Wang et al., 2009c; Xu et al., 2013) and the reduction of the refrigerant temperature at compressor discharge with the related enlargement of compressor operating envelope (Joppolo et al., 2010). However, despite the advantages this kind of compressor provides, the optimal control strategy (Xu et al., 2011; Heo et al., 2012) as well as the optimal architecture (Ma and Zhao, 2008; Wang et al., 2009a; Roh and Kim, 2011, 2012; Heo et al., 2011) of a vapour compression system equipped with it is still under investigation.

In this context, the development of a mathematical model of a scroll compressor with vapour injection may be helpful in supporting the analysis of system configuration or control. Indeed, many studies available in the open literature have deserved attention to the simulation of vapour injection scroll compressor but, differently from the modelling of standard scroll compressor where three distinct modelling techniques (geometrical, semi-empirical and empirical modelling) are largely proposed (Byrne et al., 2014), for the vapour injection scroll compressor mainly geometrical models are mainly proposed with few exceptions as discussed below.

Park et al. (2002) developed a deterministic model of a variable speed scroll compressor with vapour injection working with R22. The model was validated considering only the no injection condition showing deviations of the predicted compressor capacity and electrical power lower than 10% with respect to the experimental ones. The model was then used to investigate the influence of geometrical (injection hole diam-eter and position) and thermodynamic (refrigerant pressure and quality or superheat) injection parameters on compressor working parameters as function of rotational frequency. An optimal configuration leading to an increase of COP equal to 12% COP was found.

Winandy and Lebrun (2002) developed a semi-empirical model of a fixed speed scroll compressor with refrigerant injection working with R22. The semi-empirical model was able to calculate the refrigerant mass flow rate, the compressor electrical power and the refrigerant temperature at compressor discharge. The validation was carried out considering the no injection condition, the vapour injection condition and the liquid injection condition showing deviations of the predicted refrigerant mass flow rate in the range −4.5% − +4% (with the exception of one liquid injection point where the deviation was +13.5%), of the compressor electrical power in the range −4.5% − +4.5% and of the refrigerant temperature at compressor discharge in the range −5 K − +5 K. No information about the validation of predicted injection mass flow rate was given.

Ma and Chai (2004) developed and validated (data from Ma et al. (2003)) a thermodynamic model of the compression process inside a fixed speed scroll compressor with vapour injection working with R22. Although the model was validated only in a single working condition, the agreement between calculated and experimental data was within −1% − +6%. The model was then used to investigate the influence of refrigerant injection pressure on compressor working parameters as function of evaporating temperature. Different injection pressures for maximum heating capacity or COP were found.

Wang et al. (2008) developed and validated a deterministic model of a fixed speed scroll compressor with vapour injection working with R22. The model was validated under different working conditions showing deviations of the predicted refrigerant mass flow rate, injected mass flow rate, compressor electrical power and refrigerant temperature at compressor discharge in the range −4% − +3%. A sensitivity analysis of the model was then carried out leading to the conclusion that both the heat transfer between the scroll wraps and the refrigerant and the back-pressure pocket

configuration have very little influence and can be neglected in the modelling process. Finally, the concept of continuous "adiabatic throttling + isobaric mixing" to describe the refrigerant injection process in the scroll compressor was introduced. The same model was then used by the same authors in order to assess the influence of injection pressure and enthalpy and of injection holes area and position on compressor general performance (Wang et al., 2009b) and to find the optimal system configuration and control strategy (Wang et al., 2009a).

Cho et al. (2012) developed a simplified deterministic model of a variable speed scroll compressor with vapour injection in symmetric and asymmetric scroll compressors. The model was firstly validated under different working conditions and rotational frequencies obtaining an agreement between calculated and experimental heating capacity within ±10%. The analysis of the optimum injection hole diameter and angle in symmetric and asymmetric scroll compressors was afterwards carried out finding that the optimal injection hole angle in both geometries is lower than 360° and that injection hole diameter should increase as the rotational frequency increases.

Qiao et al. (2015a) developed a transient, lumped model of a fixed speed scroll with vapour injection working with R410A. The compression process is simulated introducing a polytropic process, whose index is estimated on the basis of experimental results, and the model needs 8 curve fitting constants to simulate the compressor. The model is then integrated in a transient model of an air-to-air heat pump and successfully validated (Qiao et al., 2015b).

All the previous papers provide valuable models of scroll compressor with vapour injection. However, with the exceptions of the work of Winandy and Lebrun (2002) and Qiao et al. (2015a), all the models are deterministic, requiring a detailed description of the compressor geometry as an input to simulate compressor operation. On the other hand, the semi-empirical model of Winandy and Lebrun (2002) does not need the compressor geometry to predict its performance but does not allow to compute injection mass flow rate or to deal with rotational frequency variation, whereas the model of Qiao et al. (2015a) needs to introduce correlations deduced from compressor performance map to compute compressor power input. Therefore, the purpose of this paper is to update the original semi-empirical model proposed by Winandy and Lebrun (2002) to account for injection mass flow rate prediction and rotational frequency variation. The final model is a reliable model able to accurately predict compressor macroscopic performance (suction and injection mass flow rates, compressor electrical power and refrigerant temperature at compressor discharge) and to be integrated in vapour compression system simulation without a deep knowledge of the compressor geometrical features.

## 2. Model description

As stated, the model proposed by Winandy and Lebrun (2002) is the basis for the development of the thermodynamic model of the variable speed scroll compressor with vapour injection. The original model decomposes the process of the refrigerant inside the compressor into four steps, putting the injection mass flow rate at compressor suction and neglecting internal leakage, heat transfer to scroll wraps, suction and discharge pressure drop and rotational frequency variation. In the present model, both pressure drop and heat transfer (Wang et al., 2008) are still neglected whereas further steps are added to the evolution of the refrigerant inside the compressor in order to account for refrigerant leakage and vapour injection. The refrigerant process is shown in Fig. 1 and consists of the following steps:

1. Isobaric heating at compressor suction (SUC → 1).
2. Isobaric mixing with internal leakage (1 → 2).
3. First isentropic compression up to the first intermediate pressure (2 → 3).
4. First isobaric mixing with the first injection mass flow rate (3 → 5).
5. Second isentropic compression up to the second intermediate pressure (5 → 6).
6. Second isobaric mixing with second injection mass flow rate (6 → 8).
7. Third isentropic compression up to adapted conditions (8 → ADP).
8. Adiabatic compression at constant machine volume up to discharge pressure (ADP → 9).
9. Isobaric cooling from scroll outlet to compressor discharge (9 → DIS).

As shown in Fig. 1, the vapour injection scroll compressor is modelled considering four Virtual Compressors (VC), instead of the two proposed in the original model, and two injection lines, instead of the only one that physically exists in the real compressor considered in this study schematically depicted Fig. 2. Although quite complex, this choice arises from the need of accurately describing the actual process of refrigerant compression and injection. Indeed, as pointed out by the numerical study of Cho et al. (2012) and confirmed by our in-house experimental tests, the injection mass flow rate is not a constant parameter but it strongly varies as function of orbiting angle as qualitatively shown in Fig. 3 (a) (continuous line). The main driver of injection mass flow rate is the pressure difference between the injection line and the compression pocket. This pressure difference is not constant but reaches its maximum value just after the injection holes uncovering (Fig. 3(b), continuous line), inducing a great amount of refrigerant to be pushed inside the compression pocket. The pocket then begins to be filled with injected refrigerant but, in the meanwhile, orbiting scroll rotation continues, increasing the refrigerant pressure inside the pocket and reducing pocket-to-injection pressure difference. The pressure in the compression pocket keeps on increasing until it becomes greater than the injection pressure, triggering a back-flow phenomenon where the refrigerant flows out from the compression pocket to the injection line. The process ends as soon as the injection holes are covered by the orbiting scroll. In the present model, the continuous "compression + injection process" is approximated with a lumped parameter approach introducing two steps at constant pressure, with increasing pressure from the first to the second, that represent two successive average intermediate

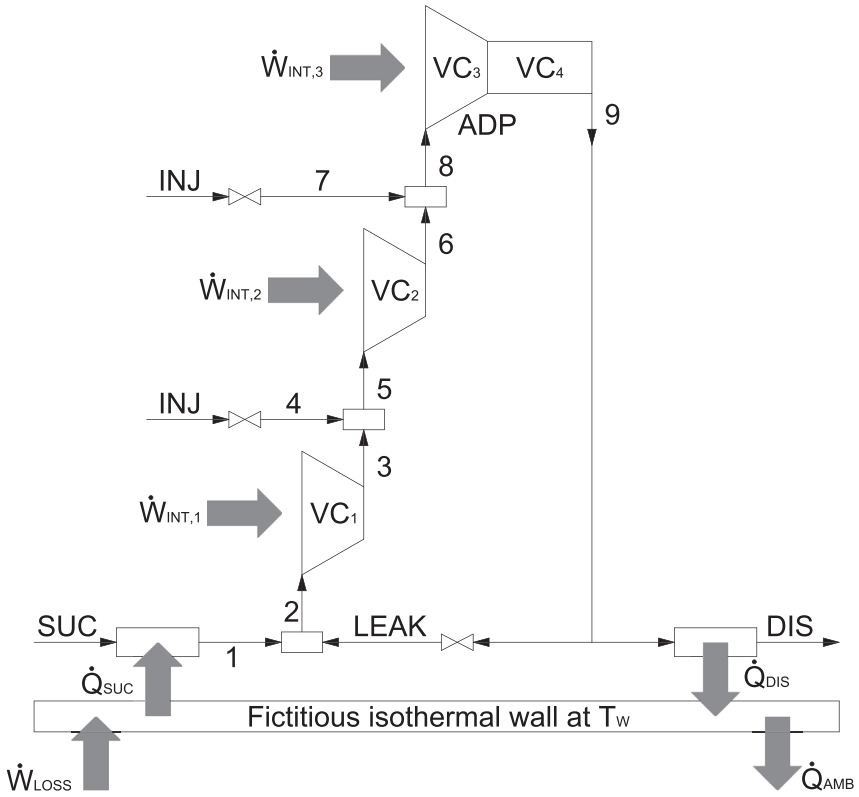


**Fig. 1 – Schematic diagram of the proposed compressor model.**

pressure conditions of the refrigerant inside the compression pocket during the "compression + injection process" (Fig. 3(b), dashed line). Consequently, two different injection mass flow rate are calculated (Fig. 3(a), dashed line) as function of the pressure inside the compression pocket at that particular step and the overall injection mass flow rate becomes the algebraic sum of them. It is worth specifying that adopted pressure schematic shown in Fig. 3(a) is only representative, being both intermediate pressures not constant but adjusted by the model as function of the compressor working conditions. Therefore, although the first intermediate pressure is always lower than the injection one, the second intermediate pressure computed by the model could be greater, equal or lower than the injection one, leading to ejection or injection of refrigerant from or into the compression pocket as shown further in Section 3. Therefore, three Virtual Compressors are used to simulate the "compression + injection process" that occurs from the refrigerant suction to the injection holes closure. Among them, $VC_1$ is used to describe the suction of the refrigerant and its first compression until the first intermediate pressure where the first injection happens. This process physically represents the first part of the

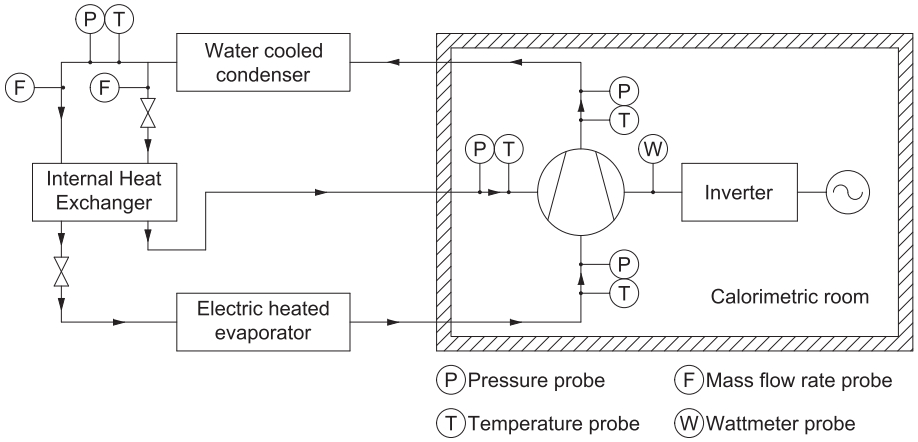


**Fig. 2 – Schematic diagram of the calorimetric room and experimental set-up.**

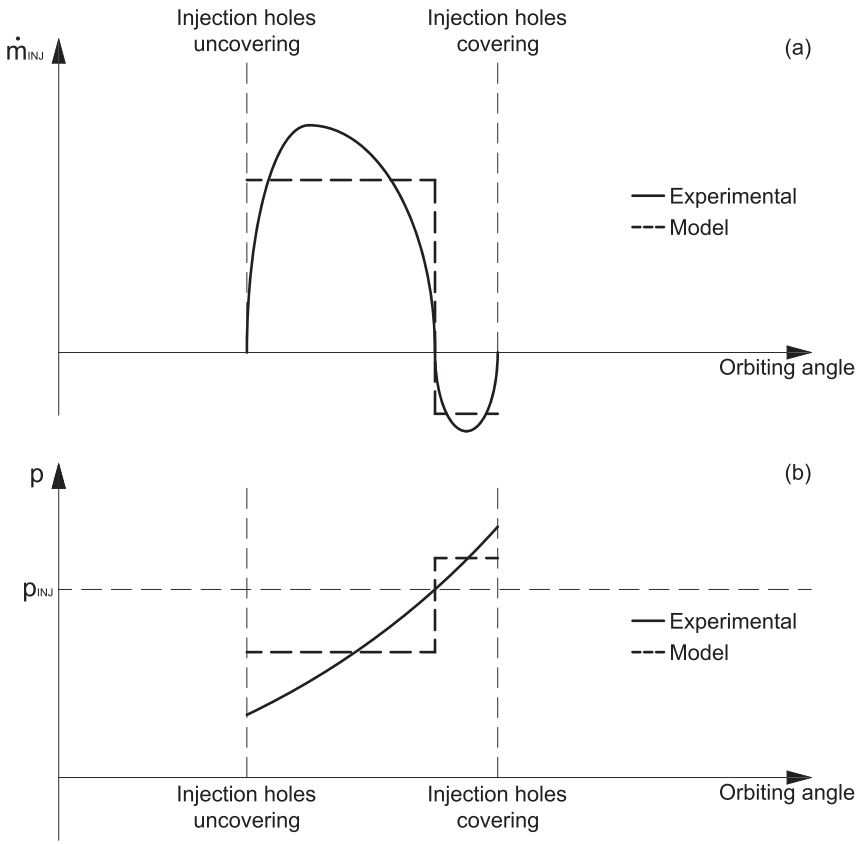


**Fig. 3 – Injection mass flow rate (a) and compression pocket pressure (b) evolution as a function of orbiting angle (adapted from Maggioni and Proserpio (2013)).**

"compression + injection process", where, after suction port closure, injection holes uncover and injection flow rate fills the compression pocket and mixes with the refrigerant in it. After the mixing process, the refrigerant is sucked by $VC_2$ that is used to simulate the second part of the "compression + injection process", where the pocket pressure could overcome the injection pressure triggering back-flow phenomenon. As stated, the second intermediate pressure is adjusted by the model and could be greater, equal or lower than the injection pressure (pressure levels shown in Fig. 3(b) are only representative of the lumped parameter approach considered in the model). The mixed refrigerant is then sucked by $VC_3$ which is introduced to account for the compression process that happens after injection holes closure up to adapted conditions, which are the conditions imposed by the fixed geometry of the volumetric scroll compressor under consideration. Finally, $VC_4$ is introduced to describe the compressor chamber opening to the discharge plenum and to account for under- or over-compression losses, according to the original model.

The equations that apply to each step are detailed hereinafter, keeping in mind that mass and energy balances are always valid but are explicitly reported only when needed.

### 2.1. *Isobaric heating at compressor suction*

The heat transfer at the compressor suction is accounted for with the same approach proposed in the original model. Indeed, a fictitious isothermal wall is introduced to describe compressor casing with a lumped parameter assuming that it is able to represent all the heat transfer modes inside the compressor (namely suction heating, electromechanical losses heating, discharge cooling and compressor to ambient thermal losses). The following equations apply for the isobaric heating process:

$$\dot{Q}_{SUC} = \dot{m}_{SUC}(h_1 - h_{SUC}) = \varepsilon_{SUC}\dot{m}_{SUC}c_{P,SUC}(T_W - T_{SUC}) \quad (1)$$

$$\varepsilon_{SUC} = 1 - e^{-NTU_{SUC}} \quad (2)$$

$$NTU_{SUC} = \frac{1}{\dot{m}_{SUC}c_{P,SUC}}(UA)_{SUC,REF}\left(\frac{\dot{m}_{SUC}}{\dot{m}_{REF}}\right)^{0.8} \quad (3)$$

Eq. (3) is used to account for the variation of the overall heat transfer coefficient as a function of refrigerant mass flow rate according to the Reynolds heat transfer analogy where the exponent 0.8 is chosen as representative of a fully developed turbulent flow. The parameter $(UA)_{SUC,REF}$ is the reference overall heat transfer coefficient at the refrigerant suction and is a parameter of the model.

### 2.2. *Isobaric mixing with internal leakage*

All the internal leakages (flank and radial) that occur continually in the compressor as the compression proceed are modelled using a lumped parameter approach that, for the

sake of simplicity, considers them to happen at the suction of $VC_1$ and at the discharge of $VC_4$ as shown in Fig. 1. The following equations are used to describe the isobaric mixing with internal leakage and to compute the refrigerant mass flow rate sucked by $VC_1$:

$$\dot{m}_2 = \dot{m}_{SUC} + \dot{m}_{LEAK} = \rho(p_2, h_2)\dot{V}_{VC_1} = \rho(p_2, h_2)V_{VC_1}f \tag{4}$$

$$\dot{m}_2 h_2 = \dot{m}_{SUC} h_1 + \dot{m}_{LEAK} h_9 \tag{5}$$

In Eq. (4) $V_{VC_1}$ is the swept volume at the compressor suction, which is a parameter of the model. On the other hand, the leakage mass flow rate is modelled with reference to the isentropic flow of a compressible gas through a simply convergent nozzle (Lemort, 2008; Giuffrida, 2014) according to the following equation:

$$\dot{m}_{LEAK} = \rho\left(p_{THR,LEAK}, s_9\right) A_{LEAK}\sqrt{2\left[h_9 - h\left(p_{THR,LEAK}, s_9\right)\right]} \tag{6}$$

In Eq. (6) $A_{LEAK}$ represents the cross sectional area of the leakage nozzle throat and is a parameter of the model, whereas the calculation of the throat pressure $p_{THR,LEAK}$ is carried out considering the leaked refrigerant as a perfect gas and taking the maximum between the actual pressure at nozzle outlet and the critical pressure:

$$p_{THR,LEAK} = max\left[p_1, p_{CRIT,LEAK}\right] = max\left[p_1, p_9\left(\frac{2}{\gamma_9 + 1}\right)^{\frac{\gamma_9}{\gamma_9 - 1}}\right] \tag{7}$$

Eq. (7) is introduced in order to consider that, depending on compressor operating conditions, chocked flow may occur in the nozzle throat since the ratio between actual inlet nozzle pressure to actual nozzle discharge pressure could be greater than the critical one.

### 2.3. First isentropic compression up to the first intermediate pressure and isobaric mixing with the first injection mass flow rate

In the proposed model, the first compression that the refrigerant undergoes in $VC_1$ is considered isentropic as done in the original model and has to be treated together with the first injection mass flow rate calculation and the subsequent mixing process. The reason is that, as previously stated, the first injection process is supposed to happen at a first intermediate pressure that physically represents an average value of the pressure in the compression pocket during the first part of the injection process. This intermediate pressure influences, at one time, the state of the refrigerant that is compressed from suction to intermediate pressure (state 3), the state of the injected refrigerant together with its mass flow rate (state 4), the state of mixed conditions (state 5) and, as a consequence, the amount of refrigerant held in the compression pocket at that particular stage of the compression + injection process. Therefore, intermediate pressure is not known a priori but depends on the state of sucked and injected refrigerant and on the geometry of the compression pocket that imposes a maximum allowable mass flow rate. The following equations are solved to identify the intermediate pressure and to compute first injection mass flow rate and mixed conditions:

$$\dot{m}_5 = \dot{m}_3 + \dot{m}_4 = \rho(p_5, h_5)\dot{V}_{VC_2} = \rho(p_5, h_5)V_{VC_2}f \tag{8}$$

$$\dot{m}_5 h_5 = \dot{m}_3 h_3 + \dot{m}_4 h_{INJ} \tag{9}$$

$$\dot{m}_4 = \rho\left(p_{THR,INJ,4}, s_{INJ}\right) A_{INJ}\sqrt{2\left[h_{INJ} - h\left(p_{THR,INJ,4}, s_{INJ}\right)\right]} \tag{10}$$

$$p_{THR,INJ,4} = max\left[p_4, p_{CRIT,INJ}\right] = max\left[p_4, p_{INJ}\left(\frac{2}{\gamma_{INJ} + 1}\right)^{\frac{\gamma_{INJ}}{\gamma_{INJ} - 1}}\right] \tag{11}$$

$VC_2$ in Eq. (8) is the swept volume of the Virtual Compressor 2. This is not a parameter of the model but it is calculated as the mean value between $VC_1$ and $VC_3$. As shown by Equations 10 and 11, the injection mass flow rate is computed considering the isentropic flow of a perfect gas in a simply convergent nozzle, as done for the leakage mass flow rate, where $A_{INJ}$ stands for the cross sectional area of the injection nozzle throat and is a parameter of the model.

Once the refrigerant states and the first injection mass flow rate are calculated, the first compressor internal power is computed:

$$\dot{W}_{INT,1} = \dot{m}_2(h_3 - h_2) \tag{12}$$

### 2.4. Second isentropic compression up to the second intermediate pressure and isobaric mixing with the second injection mass flow rate

The same considerations stated in the previous section apply to the second compression, the second injection mass flow rate calculation and the second mixing process. Therefore, again, these phenomena have to be treated together to identify the second intermediate pressure and to compute second injection mass flow rate. Accordingly, the equation used in the model to calculate the mass flow rate sucked by $VC_3$ is similar to Eq. (8):

$$\dot{m}_8 = \dot{m}_6 + \dot{m}_7 = \rho(p_8, h_8)\dot{V}_{VC_3} = \rho(p_8, h_8)V_{VC_3}f \tag{13}$$

In Eq. (13) $V_{VC_3}$ is the swept volume after the injection holes closure and is a parameter of the model. On the other hand, differently from the previous processes, the second intermediate pressure could be greater or lower than the injection pressure, meaning that the injection flow rate could be pushed into the compression pocket (injection flow rate) or out of it (ejection flow rate or back-flow process). In the former situation, the same set of Eqs. 9–11 apply for the calculation of intermediate pressure and injection mass flow rate (with the obvious subscript switch) whereas in the latter, Equations 9–11 have to be changed to account for refrigerant back-flow from compression pocket to injection line:

$$h_7 = h_8 = h_6 \tag{14}$$

$$\dot{m}_7 = -\rho\left(p_{THR,INJ}, s_7\right) A_{INJ}\sqrt{2\left[h_7 - h\left(p_{THR,INJ}, s_7\right)\right]} \tag{15}$$

$$p_{THR,INJ} = max\left[p_{INJ}, p_{CRIT,INJ}\right] = max\left[p_{INJ}, p_7\left(\frac{2}{\gamma_7 + 1}\right)^{\frac{\gamma_7}{\gamma_7 - 1}}\right] \tag{16}$$

The "minus" sign in Eq. (15) accounts for a back-flow from the compression pocket to the injection line. Again, once the refrigerant states and the second injection mass flow rate are

calculated, the second compressor internal power and the overall injection mass flow rate are computed:

$$\dot{W}_{INT,2} = \dot{m}_5(h_6 - h_5) \tag{17}$$

$$\dot{m}_{INJ} = \dot{m}_4 + \dot{m}_7 \tag{18}$$

### 2.5. Third isentropic compression up to the adapted conditions and adiabatic compression at constant machine volume up to the discharge pressure

Following the original model, compression in $V_{VC_3}$ is supposed to be isentropic up to the adapted conditions. These conditions are imposed by a parameter of the model, the built-in volume ratio, that is defined according to the following equation:

$$BVR = \left(\frac{\rho_{ADP}}{\rho_2}\right) \tag{19}$$

Finally, the compression in $V_{VC_4}$ is supposed to be adiabatic and at constant machine volume. This is the part of the compression process where over-compression or under-compression losses occur since the adapted pressure could be, respectively, greater or lower than compressor discharge pressure. In order to equalize the adapted pressure with the discharge one, a refrigerant flow rate has to move from the discharge plenum to the compression discharge chamber (under-compression) or vice-versa (over-compression) as soon as the two volumes are put in contact and the fluid is no more trapped. The model assumes that this phenomenon occurs instantaneously and, therefore, the following equations apply:

$$\rho_9 = \rho_{ADP} \tag{20}$$

$$\dot{W}_{INT,3} = \dot{m}_8(h_{ADP} - h_8) + \dot{m}_8\frac{(p_9 - p_{ADP})}{\rho_{ADP}} \tag{21}$$

### 2.6. Isobaric cooling from scroll outlet to compressor discharge

The same set of Equations (1)–(3) used to describe the isobaric heating applies to the discharge cooling and only the main adjustments are hereinafter reported:

$$\dot{m}_{DIS} = \dot{m}_9 - \dot{m}_{LEAK} \tag{22}$$

$$\dot{Q}_{DIS} = \dot{m}_{DIS}(h_9 - h_{DIS}) = \varepsilon_{DIS}\dot{m}_{DIS}c_{P,9}(T_9 - T_W) \tag{23}$$

$$NTU_{DIS} = \frac{1}{\dot{m}_{DIS}c_{P,9}}(UA)_{DIS,REF}\left(\frac{\dot{m}_{DIS}}{\dot{m}_{REF}}\right)^{0.8} \tag{24}$$

The parameter $(UA)_{DIS,REF}$ in Eq. (24) is the reference overall heat transfer coefficient at the refrigerant discharge and is a parameter of the model.

### 2.7. Electro-mechanical losses, ambient losses and closure equations

The overall compressor electrical power input is equal to the sum of the compressor internal power plus the electro-mechanical losses:

$$\dot{W}_{COMP} = \dot{W}_{REF} + \dot{W}_{LOSS} \tag{25}$$

The first term is the mechanical power given to the refrigerant and is computed by the following equation:

$$\dot{W}_{REF} = \dot{W}_{INT,1} + \dot{W}_{INT,2} + \dot{W}_{INT,3} \tag{26}$$

On the other hand, electromechanical losses are computed updating the formulation proposed by Lemort (2008) with the introduction of a term that represents the dependence of electromechanical losses on compressor rotational frequency (torque losses):

$$\dot{W}_{LOSS} = \alpha_{LOSS}\dot{W}_{REF} + \dot{W}_{LOSS,REF}\left(\frac{f}{f_{REF}}\right) \tag{27}$$

In Eq. (27), $\alpha_{LOSS}$ is the coefficient of proportionality between electro-mechanical losses and compressor internal power and $\dot{W}_{LOSS,REF}$ is the reference electro-mechanical loss related to torque loss but expressed in term of power. Both are model parameters.

Compressor to ambient thermal losses are calculated using the following equation:

$$\dot{Q}_{AMB} = (UA)_{AMB}(T_W - T_A) \tag{28}$$

$(UA)_{AMB}$ in Eq. (28) is the overall heat transfer coefficient between the compressor casing and the surrounding and is a parameter of the model that is kept constant in every working condition.

Finally, a steady-state heat balance on the fictitious wall is used as closure equation:

$$\dot{W}_{LOSS} + \dot{Q}_{DIS} - \dot{Q}_{AMB} - \dot{Q}_{SUC} = 0 \tag{29}$$

Overall, the model needs 10 parameters to simulate the variable speed scroll compressor with vapour injection and to calculate the compressor macroscopic performance such as suction mass flow rate, injection mass flow rate, compressor electrical power and refrigerant temperature at compressor discharge. In addition, suction pressure and temperature, injection pressure and temperature, discharge pressure and rotational frequency have to be supplied to the model as compressor working conditions.

## 3. Results and discussion

63 experimental tests were carried out in a calorimetric room designed to comply with European Standard EN 13771 (EN 13771, 2003) for compressor testing and whose schematic is shown in Fig. 2. The tested compressor is a hermetic, variable speed scroll compressor with vapour injection working with R-410A and POE oil and whose swept volume is equal to 5.3 $m^3\ h^{-1}$ at 50 Hz. Instrumentation uncertainty is shown in Table 1, whereas test conditions are provided in Table 2. Experimental results are gathered in Table A.1 in Appendix A and they are not discussed in detail since the objective of the paper is to present and validate the model.

The model described in previous section is implemented in MATLAB environment using REFPROP 9.1 (Lemmon et al., 2013) to compute the refrigerant properties. The parameters of the model are identified by minimizing the following objective function that express the relative error between

**Table 1 – Instrumentation and related uncertainty.**

| Variable | Device type | Uncertainty |
|---|---|---|
| Mass flow rate | Coriolis flowmeter | ±1% |
| Pressure | Strain gauge | ±0.2% f.s. |
| Temperature | Pt100 | ±0.15 K |
| Electrical power | Power meter | ±1% |

**Table 2 – Test conditions.**

| Variable | Range |
|---|---|
| Suction pressure | 330–1250 kPa |
| Suction superheating | 9.8–10.3 K |
| Injection pressure | 607–2325 kPa |
| Injection superheating | 4.4–10.1 K |
| Discharge pressure | 1550–4450 kPa |
| Rotational frequency | 40–116.67 Hz |
| Ambient temperature | 308.15 K |

measured and calculated quantities ($n$ is the number of experimental points):

$$g = \sqrt{\frac{1}{n}\sum_{i=1}^{n}\left[\left(1-\frac{\dot{m}_{SUC,CALC,i}}{\dot{m}_{SUC,EXP,i}}\right)^2+\left(1-\frac{\dot{m}_{INJ,CALC,i}}{\dot{m}_{INJ,EXP,i}}\right)^2+\left(1-\frac{\dot{W}_{CALC,i}}{\dot{W}_{EXP,i}}\right)^2+\left(1-\frac{T_{DIS,CALC,i}}{T_{DIS,EXP,i}}\right)\right]^2} \quad (30)$$

The minimization process is carried out using optimization routine, available in MATLAB Optimization Toolbox and specifically dedicated to multivariable function minimization, giving particular care to the check that the final set of parameters lead to the global minimum of function $g$. Prior to the minimization process, references of refrigerant mass flow rate and rotational frequency have to be set. The reference refrigerant mass flow rate is chosen multiplying the swept volume by the vapour density of saturated refrigerant at 273.15 K, whereas the grid frequency is used for the reference rotational frequency. Therefore, the two reference values are $\dot{m}_{REF} = 0.045$ kg s$^{-1}$ and $f_{ROT,REF} = 50$ Hz. The parameters obtained at the end of the identification procedure are shown in Table 3.

The identified swept volume is 1.5% higher than the geometrical one. This could be explained by the supercharging effect described by Nieter (1988) that is the refrigerant at the suction begins to be compressed before the end of the suction process due to the volume reduction of suction pockets near the end of it. On the other hand, the identified *BVR* is equal to 3.34 which is typical for compressor designed for high temperature lift application such the one used in the experimental campaign.

**Table 3 – Identified parameters of the model.**

| Parameter | Value |
|---|---|
| $UA_{SUC,REF}$ | 6.88 W K$^{-1}$ |
| $A_{LEAK}$ | 3.36 10$^{-8}$ m$^2$ |
| $V_{VC_1}$ | 2.99 10$^{-5}$ m$^3$ |
| $A_{INJ}$ | 1.90 10$^{-6}$ m$^2$ |
| $V_{VC_3}$ | 2.06 10$^{-5}$ m$^3$ |
| BVR | 3.34 |
| $UA_{DIS,REF}$ | 1.20 W K$^{-1}$ |
| $UA_{AMB}$ | 23.66 W K$^{-1}$ |
| $\dot{W}_{LOSS,REF}$ | 386 W |
| $\alpha_{LOSS}$ | 5.96 10$^{-2}$ |

The comparison of the experimental values of the suction, injection and discharge mass flow rate with the calculated ones is shown in Fig. 4, Fig. 5 and Fig. 6 respectively. The prediction of the suction mass flow rate is very satisfactory since 62 values are predicted in the ±5% range and the error spans the range −4.40% – +6.75% where the highest or lowest value are in correspondence of experimental points taken near the envelope boundaries. On the other hand, the pre-diction of the injection mass flow rate is slightly less accurate since 35 values are calculated in the ±5% range that become 56 if the range is broadened to ±10% (only this boundary is shown in Fig. 5), being the error interval equal to −12.84% – +14.11%. Consequently, in order to improve the prediction of injection mass flow rate, further Virtual Compressors have to be added in the model, but this is left to future improvement. The impact of this less accurate prediction of injection mass flow rate on the prediction of the discharge mass flow rate is less significant since 58 values are predicted in the ±5% range and the error spans the range −5.92% – +7.75%. It is worth noting that there is a slight tendency for the model to underestimate the experimental values of suction mass flow rates in the

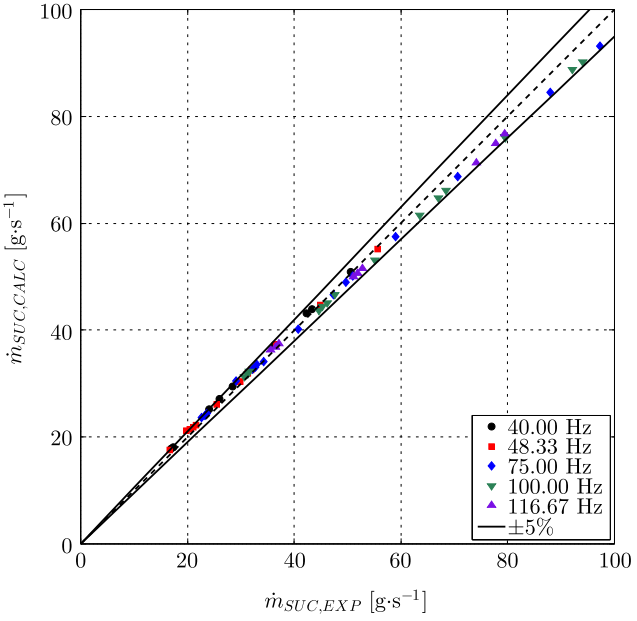


**Fig. 4 – Parity plot of suction mass flow rate.**

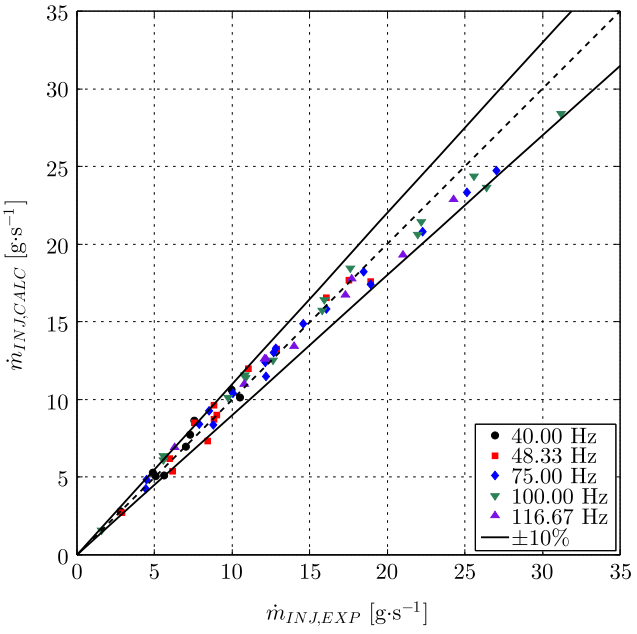


**Fig. 5 – Parity plot of injection mass flow rate.**

region of high values of it and to overestimate in the region of low ones. The reason for this behaviour is related to the position of the experimental points inside the compressor envelope. Indeed, every time the evaporation pressure (temperature) in close to the higher envelope boundary, the model tends to underestimate the refrigerant mass flow rate, whereas the opposite happens when the evaporation pressure (temperature) is close to the lower boundary. As an example, Run 49 is the run where the error in predicting suction mass flow rate reaches its minimum. Suction pressure is 930 kPa, which correspond to a saturation temperature of 278.15 K that is the maximum allowed by the compressor envelope at 100 Hz. On the other hand, Run 17 is the run where the error in predicting suction mass flow rate gets its maximum. Suction pressure is 380 kPa, which correspond to a saturation temperature of 252.15 K that is the minimum allowed by the compressor envelope at 40 Hz.

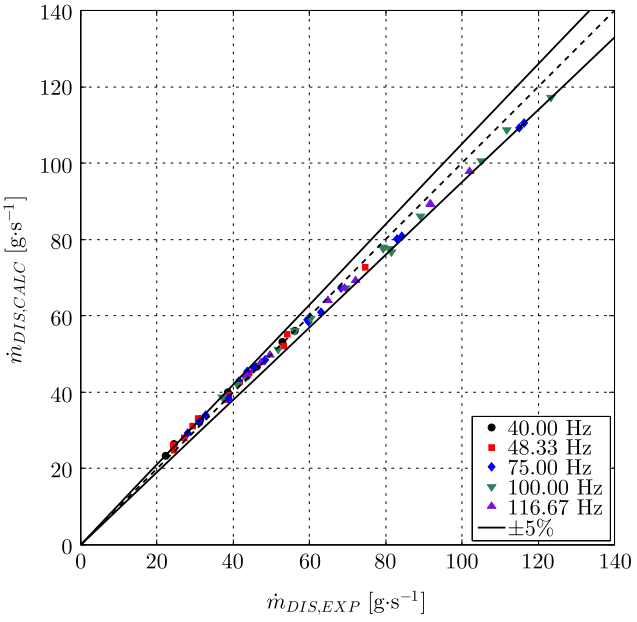


**Fig. 6 – Parity plot of discharge mass flow rate.**

As described in Sec. 2, the present model introduces two virtual compressors to approximate in a discrete way the continuous "compression + injection process" and, consequently, two different injection mass flow rates are calculated during the compressor simulation. More details about the first and the second injection mass flow rate predicted by the model are given in Fig. 7 where their value is reported for four selected compressor working conditions that, in pairs, share the same operating pressures and temperatures but not the rotational frequency (see data in Table A.1). The first injection mass flow rate ($\dot{m}_4$ in Fig. 1) computed by the model is always positive, meaning that the refrigerant is always entering in the compression pocket, and increases as the rotational frequency increases (compare Run 11 to Run 26 and Run 15 to Run 31). On the other hand, the second injection mass flow rate ($\dot{m}_7$ in Fig. 1) could be either negative, meaning that the refrigerant is exiting from the compression pocket, or positive, meaning that the refrigerant is injected into the compression pocket, depending on operating pressures, temperatures and rotational frequency. The second injection mass flow rate could change its sign either when the operating pressures and temperatures are modified but the rotational frequency is kept constant (Run 11 and Run 15) or when the operating condi-tions are kept constant but the rotational frequency is increased (Run 11 and Run 26). Finally, when the second injection mass flow rate is positive, it increases as the rotational frequency increases (Run 26 and Run 31).

The comparisons between the measured and the calculated compressor electrical power and refrigerant temperature at compressor discharge are shown in Fig. 8 and Fig. 9 respectively. According to these results, the predictions of the model are in very good agreement with the experimental data since 59 values of the compressor electrical power are

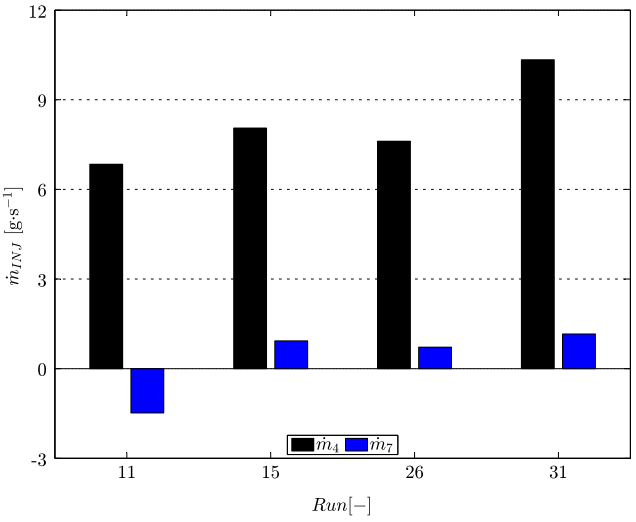


**Fig. 7 – Bar plot of first and second injection mass flow rate for four selected working conditions.**

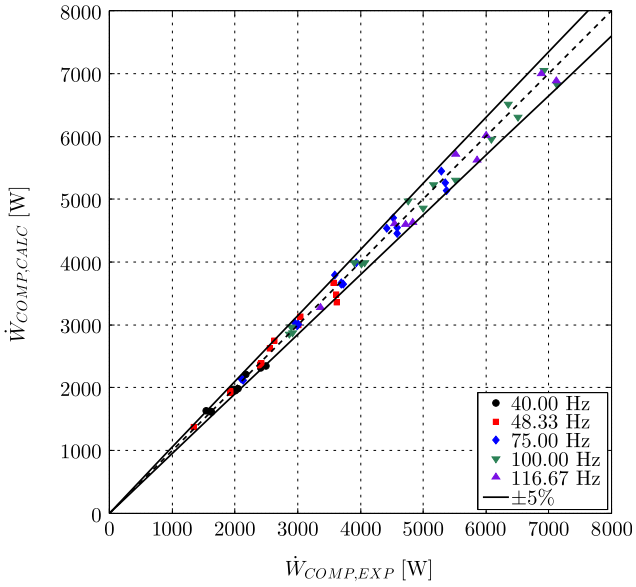


**Fig. 8 – Parity plot of the compressor electrical power.**

predicted within the ±5% range with error that spans the interval −7.46% – +6.06%, whereas 56 values of the refrigerant temperature at compressor discharge are predicted within the ±5 K range with error range equal to −9.13 K – +6.12 K. These results confirm again that the impact of the less accurate prediction of injection mass flow rate has negligible influence on compressor macroscopic performance.

Following Cuevas et al. (2010), a sensitivity analysis of the model is proposed. The sensitivity analysis is carried out varying each of the identified parameters in the range ±5%, calculating the relative error according to Eq. (30) and normalizing it with the minimum error obtained with the identified parameters collected in Table 3. The results are

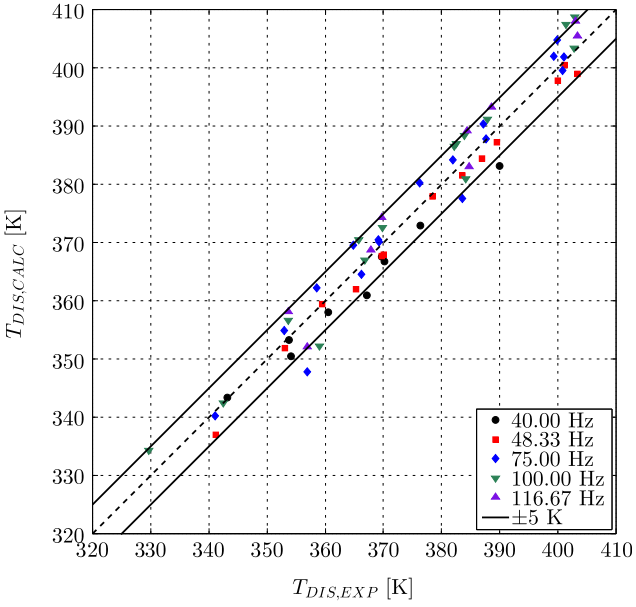


**Fig. 9 – Parity plot of the refrigerant temperature at compressor discharge.**

shown in Fig. 10, where it is possible to deduce that the model is quite sensitive to $V_{VC_1}$ and $V_{VC_3}$ and, to a less extent, to $A_{INJ}$ and $BVR$ whereas the other parameters are less influencing. Finally, since all lines depicted in Fig. 10 have their minimum when the abscissa is equal to 1, the sensitivity analysis demonstrates that the set of parameters provided in Table 3 lead to the global minimum of relative error function defined in Eq. (30).

Finally, it is worth specifying that the analysis carried out in this Section demonstrates that the model is able to accurately predict the performance of a variable speed scroll compressor with vapour injection whose swept volume is equal to 5.3 m 3 $h^{-1}$ at 50 Hz and working with R-410A since the experimental data used to identify the model parameters are available for it. However, if the performance of compressors whose size or working fluid are different from the ones considered in the present study have to be estimated, the procedure proposed by Byrne et al. (2014) can be reliably used to adapt the model parameters shown in Table 3 to the new size or the new refrigerant.

## 4. Conclusions

A semi-empirical model of a variable speed scroll compressor with vapour injection is introduced in this paper. Being a thermodynamic model, a detailed knowledge of compressor geometry is not required but 10 parameters are needed to model the process that the refrigerant undergoes from suction and injection ports to discharge port. The parameters of the model are identified through a fitting procedure that minimizes the relative error between experimental and calculated data. The model computes the suction and injection refrigerant mass flow rates, the compressor electrical power and the refrigerant temperature at the compressor discharge once the compressor working conditions and the model parameters are known. The model shows good accuracy since 89%–98% of calculated data are within ±5%, ±10% or ±5 K over a basis of 63 experimental data. As a result, the model can be reliably integrated in vapour compression system simulation for design or operating analysis.

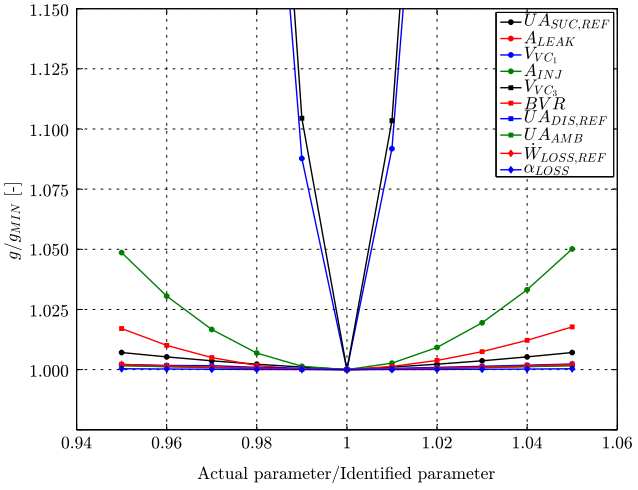


**Fig. 10 – Sensitivity analysis of the compressor model to the identified parameters.**

## Appendix. Experimental results

**Table A.1 Experimental results.**

| Working conditions | | | | | Experimental results | | | | | |
|---|---|---|---|---|---|---|---|---|---|---|
| Run | $f$ | $p_{SUC}$ | $T_{SUC}$ | $p_{INJ}$ | $T_{INJ}$ | $p_{DIS}$ | $\dot{m}_{SUC}$ | $\dot{m}_{INJ}$ | $\dot{W}_{COMP}$ | $T_{DIS}$ |
| | [Hz] | [kPa] | [K] | [kPa] | [K] | [kPa] | [kg s$^{-1}$] | [kg s$^{-1}$] | [W] | [K] |
| 1 | 40.00 | 460 | 267.15 | 902 | 283.85 | 2410 | 17.31 | 4.89 | 1616.96 | 367.14 |
| 2 | 40.00 | 680 | 278.05 | 1204 | 294.82 | 2410 | 26.06 | 5.06 | 1623.09 | 354.09 |
| 3 | 40.00 | 1080 | 293.15 | 1654 | 307.39 | 2410 | 43.29 | 2.81 | 1540.30 | 343.19 |
| 4 | 40.00 | 640 | 276.45 | 1262 | 296.46 | 3050 | 24.06 | 7.30 | 2044.25 | 370.14 |
| 5 | 40.00 | 930 | 288.15 | 1636 | 306.78 | 3050 | 36.40 | 7.02 | 2012.62 | 360.55 |
| 6 | 40.00 | 1250 | 298.15 | 1993 | 315.26 | 3050 | 50.52 | 5.62 | 1962.42 | 353.80 |
| 7 | 40.00 | 460 | 267.15 | 1039 | 288.90 | 3280 | 16.88 | 7.55 | 2178.40 | 389.99 |
| 8 | 40.00 | 750 | 281.15 | 1533 | 304.26 | 3580 | 28.52 | 9.98 | 2414.23 | 376.33 |
| 9 | 40.00 | 1080 | 293.15 | 1977 | 314.84 | 3740 | 42.31 | 10.48 | 2489.33 | 369.77 |
| 10 | 48.33 | 460 | 267.15 | 768 | 278.25 | 1560 | 21.54 | 2.89 | 1349.73 | 341.18 |
| 11 | 48.33 | 460 | 267.15 | 897 | 283.37 | 2410 | 21.15 | 5.97 | 1928.25 | 365.30 |
| 12 | 48.33 | 680 | 278.15 | 1185 | 294.07 | 2410 | 32.00 | 6.14 | 1926.36 | 353.12 |
| 13 | 48.33 | 640 | 276.45 | 1246 | 296.02 | 3050 | 29.90 | 8.83 | 2406.86 | 370.05 |
| 14 | 48.33 | 640 | 276.45 | 1255 | 296.27 | 3050 | 29.69 | 9.00 | 2420.91 | 369.73 |
| 15 | 48.33 | 930 | 288.05 | 1609 | 306.16 | 3060 | 44.87 | 8.41 | 2400.52 | 359.51 |
| 16 | 48.33 | 460 | 267.15 | 1031 | 289.14 | 3270 | 20.43 | 8.84 | 2553.93 | 386.92 |
| 17 | 48.33 | 380 | 262.15 | 875 | 282.37 | 3420 | 16.68 | 7.55 | 2626.13 | 403.41 |
| 18 | 48.33 | 460 | 266.95 | 1136 | 292.72 | 3820 | 19.82 | 11.04 | 3041.77 | 399.94 |
| 19 | 48.33 | 680 | 278.15 | 1472 | 302.87 | 3830 | 31.29 | 12.84 | 3013.71 | 383.62 |
| 20 | 48.33 | 570 | 273.15 | 1486 | 302.82 | 4450 | 25.50 | 16.07 | 3569.80 | 401.13 |
| 21 | 48.33 | 800 | 283.15 | 1811 | 311.23 | 4450 | 36.65 | 17.54 | 3615.69 | 389.47 |
| 22 | 48.33 | 1150 | 295.05 | 2259 | 320.26 | 4450 | 55.66 | 18.94 | 3623.52 | 378.48 |
| 23 | 75.00 | 330 | 258.15 | 607 | 269.25 | 1560 | 23.66 | 4.48 | 2131.79 | 356.88 |
| 24 | 75.00 | 460 | 267.15 | 785 | 278.93 | 1560 | 34.30 | 4.43 | 2099.59 | 341.13 |
| 25 | 75.00 | 330 | 258.05 | 734 | 276.35 | 2410 | 23.31 | 7.88 | 2951.67 | 383.56 |
| 26 | 75.00 | 460 | 267.15 | 927 | 285.23 | 2410 | 33.01 | 8.52 | 3007.61 | 366.23 |
| 27 | 75.00 | 680 | 278.15 | 1201 | 294.64 | 2410 | 50.93 | 8.78 | 2995.44 | 352.92 |
| 28 | 75.00 | 330 | 258.15 | 825 | 280.20 | 3050 | 22.70 | 10.07 | 3595.85 | 400.75 |
| 29 | 75.00 | 640 | 276.45 | 1266 | 296.78 | 3050 | 47.33 | 12.14 | 3696.47 | 369.09 |
| 30 | 75.00 | 640 | 276.45 | 1289 | 297.21 | 3050 | 47.37 | 12.67 | 3697.17 | 369.23 |
| 31 | 75.00 | 930 | 288.15 | 1632 | 306.59 | 3060 | 70.69 | 12.19 | 3722.60 | 358.49 |
| 32 | 75.00 | 460 | 267.15 | 1094 | 291.34 | 3270 | 32.70 | 12.82 | 3932.54 | 387.63 |
| 33 | 75.00 | 430 | 265.15 | 1149 | 293.41 | 3670 | 29.12 | 14.56 | 4424.04 | 401.02 |
| 34 | 75.00 | 460 | 266.95 | 1223 | 295.87 | 3820 | 32.26 | 16.08 | 4519.03 | 399.27 |
| 35 | 75.00 | 680 | 278.15 | 1546 | 304.38 | 3820 | 49.73 | 18.49 | 4581.97 | 381.89 |
| 36 | 75.00 | 1250 | 298.15 | 2219 | 319.54 | 3820 | 97.29 | 18.95 | 4581.49 | 364.88 |
| 37 | 75.00 | 570 | 273.15 | 1577 | 305.11 | 4450 | 40.69 | 22.29 | 5293.08 | 399.86 |
| 38 | 75.00 | 800 | 283.15 | 1898 | 313.05 | 4450 | 59.01 | 25.15 | 5354.35 | 387.14 |
| 39 | 75.00 | 1150 | 295.15 | 2325 | 321.33 | 4450 | 88.02 | 27.03 | 5369.99 | 376.22 |
| 40 | 100.00 | 770 | 282.15 | 1119 | 292.20 | 1550 | 79.55 | 1.59 | 2902.45 | 329.69 |
| 41 | 100.00 | 460 | 267.15 | 799 | 279.69 | 1560 | 46.19 | 5.58 | 2869.57 | 342.49 |
| 42 | 100.00 | 330 | 258.15 | 629 | 272.00 | 1610 | 31.55 | 5.58 | 2921.25 | 359.00 |
| 43 | 100.00 | 330 | 258.15 | 783 | 279.45 | 2410 | 31.33 | 9.75 | 3902.78 | 384.18 |
| 44 | 100.00 | 460 | 267.05 | 976 | 287.02 | 2410 | 45.23 | 10.84 | 4018.53 | 366.85 |
| 45 | 100.00 | 680 | 278.15 | 1236 | 295.84 | 2410 | 68.40 | 10.87 | 4066.06 | 353.69 |
| 46 | 100.00 | 330 | 258.15 | 912 | 284.70 | 3050 | 30.63 | 12.64 | 4758.73 | 402.82 |
| 47 | 100.00 | 640 | 276.45 | 1368 | 299.73 | 3050 | 63.46 | 15.94 | 5001.43 | 369.80 |
| 48 | 100.00 | 460 | 267.15 | 1178 | 294.67 | 3270 | 44.58 | 15.81 | 5161.88 | 387.86 |
| 49 | 100.00 | 930 | 288.15 | 1770 | 310.76 | 3400 | 94.07 | 17.63 | 5518.62 | 365.71 |
| 50 | 100.00 | 680 | 278.15 | 1638 | 306.73 | 3820 | 66.95 | 22.17 | 6081.44 | 382.47 |
| 51 | 100.00 | 500 | 269.45 | 1487 | 303.45 | 4080 | 47.65 | 21.95 | 6351.82 | 401.41 |
| 52 | 100.00 | 800 | 283.15 | 1879 | 312.56 | 4080 | 79.49 | 25.59 | 6511.18 | 382.14 |
| 53 | 100.00 | 570 | 273.15 | 1701 | 308.55 | 4450 | 55.16 | 26.39 | 6926.69 | 402.91 |
| 54 | 100.00 | 930 | 288.15 | 2181 | 319.04 | 4450 | 92.09 | 31.20 | 7130.81 | 383.87 |
| 55 | 116.67 | 330 | 258.15 | 635 | 271.58 | 1570 | 37.13 | 6.28 | 3359.84 | 356.91 |
| 56 | 116.67 | 330 | 258.15 | 814 | 280.77 | 2410 | 36.44 | 10.76 | 4545.06 | 384.73 |

***(continued)***

| Working conditions | | | | | Experimental results | | | | | |
|---|---|---|---|---|---|---|---|---|---|---|
| Run | $f$ | $p_{SUC}$ | $T_{SUC}$ | $p_{INJ}$ | $T_{INJ}$ | $p_{DIS}$ | $\dot{m}_{SUC}$ | $\dot{m}_{INJ}$ | $\dot{W}_{COMP}$ | $T_{DIS}$ |
| | [Hz] | [kPa] | [K] | [kPa] | [K] | [kPa] | [kg s$^{-1}$] | [kg s$^{-1}$] | [W] | [K] |
| 57 | 116.67 | 460 | 267.15 | 1002 | 287.69 | 2410 | 52.82 | 12.10 | 4720.80 | 367.86 |
| 58 | 116.67 | 680 | 278.15 | 1250 | 296.23 | 2410 | 79.41 | 12.19 | 4833.39 | 353.70 |
| 59 | 116.67 | 330 | 258.15 | 955 | 285.41 | 3050 | 35.63 | 13.97 | 5516.72 | 403.38 |
| 60 | 116.67 | 640 | 276.45 | 1404 | 300.86 | 3050 | 74.10 | 17.71 | 5858.55 | 369.74 |
| 61 | 116.67 | 460 | 267.15 | 1219 | 295.75 | 3270 | 51.92 | 17.28 | 6006.19 | 388.60 |
| 62 | 116.67 | 460 | 266.95 | 1375 | 300.31 | 3820 | 51.06 | 21.01 | 6884.20 | 402.97 |
| 63 | 116.67 | 680 | 278.15 | 1691 | 308.02 | 3830 | 77.71 | 24.28 | 7119.16 | 384.40 |

## REFERENCES


Byrne, P., Ghoubali, R., Miriel, J., 2014. Scroll compressor modelling for heat pumps using hydrocarbons as refrigerants. Int. J. Refrigeration 41, 1–13.

Cho, I.Y., Ko, S.B., Kim, Y., 2012. Optimization of injection holes in symmetric and asymmetric scroll compressors with vapor injection. Int. J. Refrigeration 35, 850–860.

Creux, L., 1905. Rotary engine. US Patent No. 801182.

Cuevas, C., Lebrun, J., Lemort, V., Winandy, E., 2010. Characterization of a scroll compressor under extended operating conditions. Appl. Therm. Eng. 30, 605–615.

EN 13771, 2003. Compressors and Condensing Units for Refrigeration – Performance Testing and Test Methods – Part 1: Refrigerant Compressors.

Giuffrida, A., 2014. Modelling the performance of a scroll expander for small organic rankine cycles when changing the working fluid. Appl. Therm. Eng. 70, 1040–1049.

Heo, J., Jeong, M.W., Baek, C., Kim, Y., 2011. Comparison of the heating performance of air-source heat pumps using various types of refrigerant injection. Int. J. Refrigeration 34, 444–453.

Heo, J., Kang, H., Kim, Y., 2012. Optimum cycle control of a two-stage injection heat pump with a double expansion sub-cooler. Int. J. Refrigeration 35, 58–67.

Joppolo, C., Molinaroli, L., Vecchi, G., Bianchi, C., Magni, F., Winandy, E., 2010. Performance assessment of an air-to-water R-407C heat pump with vapour injection scroll compressor. ASHRAE Trans. 116 (2), 310–317.

Lemmon, E., Huber, M., McLinden, M., 2013. NIST Standard Reference Database 23: Reference Fluid Thermodynamic and Transport Properties-REFPROP. version 9.1. National Institute of Standards and Technology, Standard Reference Data Program, Gaithersburg.

Lemort, V., 2008. Contribution to the Characterization of Scroll Machines in Compressor and Expander Modes. Ph.D. thesis. University of Liège.

Ma, G.-Y., Chai, Q.-H., 2004. Characteristics of an improved heat-pump cycle for cold regions. Appl. Energy 77, 235–247.

Ma, G.-Y., Chai, Q.-H., Jiang, Y., 2003. Experimental investigation of air-source heat pump for cold regions. Int. J. Refrigeration 26, 12–18.

Ma, G.-Y., Zhao, H.-X., 2008. Experimental study of a heat pump system with flash-tank coupled with scroll compressor. Energy Build 40, 697–701.

Maggioni, A., Proserpio, L., 2013. Development, Validation and Improvement of a Mathematical Model for an EVI Air-to-water Heat Pump through Field Test Analysis. Master's thesis. School of Industrial and Information Engineering – Politecnico di Milano.

Nieter, J., 1988. Dynamics of scroll suction process. In: Proceedings of International Compressor Engineering Conference, pp. 165–174.

Park, Y., Kim, Y., Cho, H., 2002. Thermodynamic analysis on the performance of a variable speed scroll compressor with refrigerant injection. Int. J. Refrigeration 25, 1072–1082.

Qiao, H., Aute, V., Radermacher, R., 2015a. Transient modeling of a flash tank vapor injection heat pump system – part I: model development. Int. J. Refrigeration 49, 169–182.

Qiao, H., Xu, X., Aute, V., Radermacher, R., 2015b. Transient modeling of a flash tank vapor injection heat pump system – part II: simulation results and experimental validation. Int. J. Refrigeration 49, 183–194.

Roh, C., Kim, M., 2011. Effects of intermediate pressure on the heating performance of a heat pump system using R410A vapor-injection technique. Int. J. Refrigeration 34, 1911–1921.

Roh, C., Kim, M., 2012. Comparison of the heating performance of an inverter-driven heat pump system using R410A vapor-injection into accumulator and compressor. Int. J. Refrigeration 35, 434–444.

Wang, B., Shi, W., Han, L., Li, X., 2009a. Optimization of refrigeration system with gas-injected scroll compressor. Int. J. Refrigeration 32, 1544–1554.

Wang, B., Shi, W., Li, X., 2009b. Numerical analysis on the effects of refrigerant injection on the scroll compressor. Appl. Therm. Eng. 29, 37–46.

Wang, B., Shi, W., Li, X., Yan, Q., 2008. Numerical research on the scroll compressor with refrigeration injection. Appl. Therm. Eng. 28, 440–449.

Wang, X., Hwang, Y., Radermacher, R., 2009c. Two-stage heat pump system with vapor-injected scroll compressor using R410A as a refrigerant. Int. J. Refrigeration 32, 1442–1451.

Winandy, E., Lebrun, J., 2002. Scroll compressors using gas and liquid injection: experimental analysis and modelling. Int. J. Refrigeration 25, 1143–1156.

Xu, X., Hwang, Y., Radermacher, R., 2011. Transient and steady-state experimental investigation of flash tank vapor injection heat pump cycle control strategy. Int. J. Refrigeration 34, 1922–1933.

Xu, X., Hwang, Y., Radermacher, R., 2013. Performance comparison of R410A and R32 in vapor injection cycles. Int. J. Refrigeration 36, 892–903.